ChemEngineering

MDPI

Article

Coffee Drying as a Catalytic Gas–Solid Dehydration Analogy: A Desiccant-Assisted Theoretical Framework

Eduardo Duque-Dussán [1,2]

[1] Postharvest Discipline, National Coffee Research Center–Cenicafé, km 4. Vía Antigua Chinchiná–Manizales, Manizales 170009, Colombia; eduardo.duque@cafedecolombia.com or duque_dussan@ftz.czu.cz

[2] Department of Sustainable Technologies, Faculty of Tropical AgriSciences, Czech University of Life Sciences Prague, Kamycka 129, Suchdol, 16500 Prague, Czech Republic

Abstract

Coffee drying in humid regions is frequently hindered by high rainfall and elevated relative humidity during peak harvest, prolonging drying times and risking microbial spoilage and quality deterioration. This study introduces a novel framework in which low-temperature drying is reframed as a gas–solid dehydration reaction, promoted by a catalyst analog represented by regenerable desiccants integrated into the inlet air stream to lower the humidity ratio (ΔY) and intensify the evaporation driving force. Two adsorbents, silica gel type A and zeolite 13X, were evaluated using a coupled reactor model linking fixed-bed adsorption kinetics with tensorial heat–mass transport in a 70 kg batch of parchment coffee arranged in a 0.20 m thick bed. Drying simulations from 53% to 12% (wb) at 40, 45, and 50 °C showed time reductions of 35–37% with silica gel and 44–57% with zeolite, yielding kinetic promotion factors of up to 2.3× relative to the control. Breakthrough analysis supported a dual-bed alternation strategy, with regeneration at ≤130 °C for silica and moderately higher for zeolite. A nomograph was developed to scale desiccant requirements across airflow and ΔY targets. These results confirm the feasibility and scalability of desiccant-assisted drying, providing a modular intensification pathway for farm-scale coffee processing.

Keywords: adsorption kinetics; catalytic analogy; fixed-bed design; heat–mass transfer; humidity control

Academic Editor: Mario J. Muñoz Batista

Received: 1 September 2025
Revised: 26 September 2025
Accepted: 10 October 2025
Published: 15 October 2025

Citation: Duque-Dussán, E. Coffee Drying as a Catalytic Gas–Solid Dehydration Analogy: A Desiccant-Assisted Theoretical Framework. *ChemEngineering* **2025**, *9*, 112. https://doi.org/10.3390/chemengineering9050112

1. Introduction

In tropical coffee producing regions, the peak harvesting season often coincides with extended periods of elevated rainfall and high ambient humidity, conditions that significantly hinder the removal of moisture from parchment coffee during postharvest processing [1]. The drying stage, which is essential for reducing moisture content to levels safe for storage and export, becomes particularly challenging under these circumstances, often leading to incomplete or uneven drying [2,3]. Elevated water activity (a_w > 0.70) and high moisture content during intermediate drying stages promote microbial growth and enzymatic activity, creating favorable conditions for fungal colonization and potential mycotoxin production, notably ochratoxin A (OTA) [4,5]. The presence of this contaminant is a serious food safety concern, subject to strict regulatory limits in major importing markets, and even minor exceedances can result in shipment rejections and severe economic losses [4–6]. Prolonged exposure to moist conditions also facilitates the proliferation of spoilage microorganisms, accelerates enzymatic degradation, and alters the chemical composition of the beans, affecting both volatile and non-volatile compounds [7–9]. In traditional sun

drying, which remains the predominant method among smallholder farmers, the time required to reach safe moisture levels can extend from fourteen to twenty-one days during wet seasons [10]. This extended period of exposure increases the risk of contamination, rewetting events due to nighttime condensation, and progressive biochemical degradation [11,12]. Regardless of whether the coffee is processed as washed, natural, or honey, drying consistently represents the main bottleneck in safeguarding quality and ensuring timely processing [2,12–14].

In response to these challenges, a variety of mechanical and hybrid drying systems have been developed to reduce dependence on favorable weather conditions [10,15,16]. These systems include conventional heated air dryers powered by fossil fuels such as diesel or liquefied petroleum gas, electrically driven dryers, and solar assisted designs with thermal storage [13,17–19]. While effective in maintaining continuous operation during adverse weather, they are often constrained by high capital requirements, substantial operating costs, and significant environmental impacts [10]. Fuel-based dryers require a consistent and reliable supply of combustible materials, a condition that can be difficult and costly to meet in remote rural areas [20,21]. Electrically powered systems can strain local energy infrastructure and result in high production costs in regions where electricity tariffs are elevated or supply is unstable [15]. Furthermore, many of these designs concentrate on increasing air temperature to accelerate drying but give limited attention to the psychrometric driving force, in particular the absolute humidity of the drying air, as a variable that can be deliberately controlled to enhance moisture removal [16,22]. In humid climates, even heated air may remain close to saturation, reducing the vapor pressure gradient between the beans and the surrounding air [12,23,24]. This constraint means that higher temperatures alone may not significantly improve drying efficiency, indicating a need for strategies that alter air properties without proportionally increasing thermal energy consumption.

Desiccant-assisted dehumidification is an established solution in sectors where precise humidity control is essential for maintaining product stability and process consistency [25–27]. In the pharmaceutical industry, desiccants are used to protect moisture-sensitive formulations, in food preservation they are employed to extend shelf life and prevent microbial growth, and in industrial gas processing they are used to avoid condensation and corrosion [28–33]. Common adsorbent materials such as silica gel, zeolite, and activated alumina are capable of lowering the absolute humidity of process air, thereby increasing the vapor pressure difference between the air and the wet material [34–36]. This facilitates faster moisture migration without raising air temperature, enabling shorter drying times, reduced energy consumption, and improved retention of heat-sensitive quality attributes [26,37]. Many desiccants can be regenerated with moderate heat input, allowing multiple reuse cycles and making them suitable for both centralized facilities and small-scale, decentralized operations [38–40]. Despite these advantages and their widespread use in other industries, the application of regenerable desiccants in postharvest coffee drying remains virtually unexplored. To date, there is little to no evidence of targeted research or commercial use of this technology in coffee processing, even in regions where high humidity during harvest severely limits drying efficiency, the use of desiccators has only been reported for the transport of green coffee [30].

The present work reconceptualizes coffee drying as a gas–solid dehydration process in which the moisture contained within the coffee matrix behaves as a reactant, thermodynamically driven toward the vapor phase through a reduction in the ambient humidity ratio [41,42]. In this framework, a regenerable desiccant functions analogously to a catalyst, not changing the chemical nature of the water but increasing the effective reaction rate constant by lowering the partial pressure of water vapor in the surrounding air [43,44].

This analogy supports the application of fixed-bed reactor theory, adsorption kinetics, and coupled heat and mass transfer equations to describe the integrated dynamics of air dehumidification and moisture removal from coffee [26]. Two adsorbents, silica gel type A and zeolite 13X, are evaluated for their ability to maintain low humidity ratios under airflow and temperature conditions that are representative of on-farm processing. The study combines adsorption modeling with drying simulations at inlet air temperatures of 40, 45, and 50 °C to estimate reductions in drying time, determine optimal adsorbent quantities, and develop regeneration strategies that are practical in rural contexts. By merging principles from chemical reaction engineering with postharvest coffee technology, this approach offers a low energy, modular pathway for process intensification that is scalable and adaptable to the operational realities of smallholder farms in humid tropical environments.

2. Materials and Methods

2.1. Raw Material and Initial Conditions

The "reactant" in this study was *Coffea arabica* L. var. Cenicafé 1 parchment coffee obtained from wet processing, with an initial moisture content X_0 = 53% wet basis (wb). The target final moisture content, X_f, lies in the range 10–12% (wb), consistent with international storage and quality preservation standards [45]. A batch of wet processed parchment coffee of mass m_{wet} = 70 kg was modeled, corresponding to approximately $m_{dry} \approx 34$ kg [42,46]. The coffee was arranged in a rectangular static bed of length L = 1 m, width W = 0.50 m, and thickness H_c = 0.20 m, providing a cross-section area of 0.50 m^2.

The coffee bed is conceptualized as a porous, anisotropic granular medium exhibiting coupled heat and mass transport, where the moisture content $X(r,t)$, with r denoting the spatial position vector within the bed and t the drying time, was treated as a scalar field embedded within a tensorial framework to account for direction-dependent diffusivities [47,48]. The dry solid density (ρ_s) and specific heat capacity (c_p) were taken from the literature for model parameterization [49]. For the present modeling framework, moisture diffusivity, thermal conductivity, and equilibrium isotherm parameters were adopted from representative values in the literature, recognizing that variability exists across coffee varieties and microstructures [22,49].

2.2. Desiccant Selection and Adsorption Properties

The catalyst analog is represented by two high-capacity adsorbents, silica gel type A and zeolite 13X, selected for their strong water affinity, regeneration stability, and non-toxic nature. Equilibrium adsorption is described by the Dubinin–Astakhov (D–A) equation [50,51]:

$$q_{eq}(T,\ p) = q_s \exp\left[-\left(\frac{RT\ln\left(\frac{p_0}{p}\right)}{E}\right)^n\right] \quad (1)$$

where q_{eq} = equilibrium uptake (kg $H_2O \cdot kg^{-1}$ dry adsorbent); q_s = saturation capacity (kg $H_2O \cdot kg^{-1}$); E = characteristic adsorption energy (kJ·mol^{-1}); n = structural heterogeneity parameter; p_0/p = relative vapor pressure at temperature T. Representative parameters from literature: Silica gel A: $q_s \approx 0.35$ kg $H_2O \cdot kg^{-1}$ at 25 °C and 60% relative humidity (RH), E = 5.9 kJ·mol^{-1} and n = 2.0. Zeolite 13X: $q_s \approx 0.28$ kg $H_2O \cdot kg^{-1}$, E = 8.5 kJ mol^{-1}, n = 1.4 [50–53].

The desiccant bed was configured as a fixed-bed cartridge located upstream of the coffee bed to reduce inlet humidity ratio Y_{in} while maintaining nearly constant inlet temperature T_{in}.

2.3. Reactor Configuration

The drying system was modeled as a two-stage gas–solid reactor train, as illustrated in Figure 1. Stage 1 corresponds to the adsorption reactor, in which humid air is passed through a fixed bed of desiccant under quasi-isothermal conditions to reduce its absolute humidity. Stage 2 corresponds to the coffee drying reactor, where the conditioned air stream, with reduced humidity ratio, is introduced into a fixed shallow bed of parchment coffee. This configuration enhances the vapor pressure gradient, thereby promoting moisture migration from the coffee matrix while maintaining controlled thermal conditions.

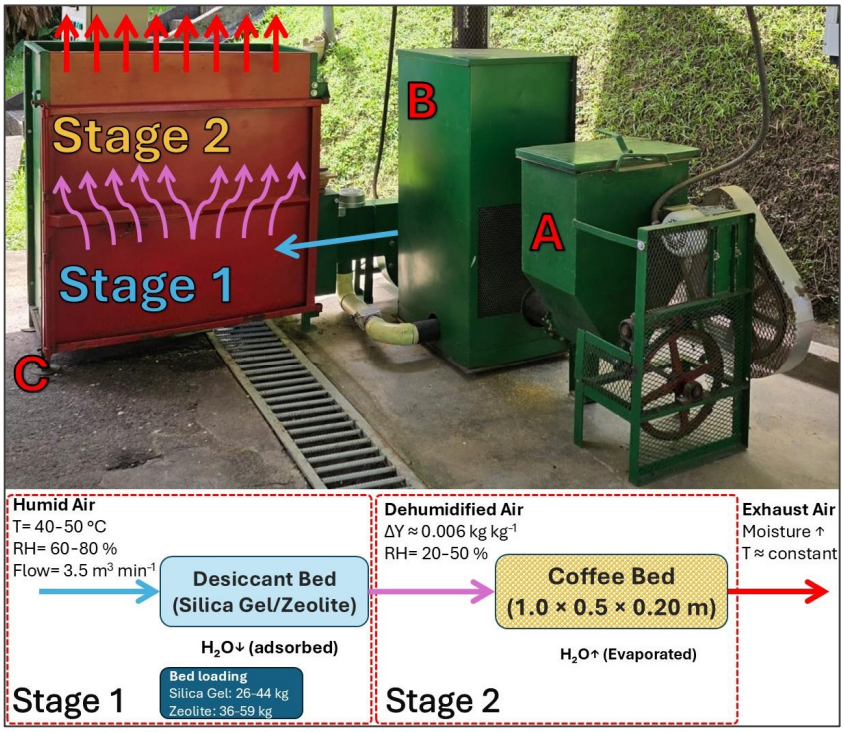

Figure 1. Desiccant-assisted coffee drying concept A Biofuel hopper (Cenicafé, Manizales, Caldas) B. Heat exchanger (Cenicafé, Manizales, Caldas). C. Dryer (Cenicafé, Manizales, Caldas). Stage 1: humid air passes through the desiccant bed where moisture is adsorbed. Stage 2: conditioned air enters the coffee bed, accelerating moisture removal.

For this theoretical outline, the desiccant bed was assumed to operate under quasi-isothermal conditions and the coffee bed under uniform airflow distribution, as necessary simplifications to establish a tractable first-principles model [36]. These assumptions provided a controlled baseline to couple adsorption kinetics with tensorial heat and mass transfer, recognizing that future work should progressively relax them to account for heterogeneity in farm-level dryers [54].

Stage I: Adsorption reactor (catalyst zone)

A fixed bed of desiccant operating under quasi-isothermal conditions [55], governed by:

$$\frac{\partial Y}{\partial z} = -\frac{K_G a_s}{G}\left[Y - Y_{eq}(T,\, q)\right] \tag{2}$$

$$\frac{\partial q}{\partial t} = k_a\left[Y - Y_{eq}(T,\, q)\right] \tag{3}$$

where K_G is the overall gas-phase mass transfer coefficient, as the specific surface area, G the mass flux of air, k_a the intraparticle adsorption rate constant, and Y_{eq} the equilibrium humidity ratio from the D-A isotherm.

Stage II: Coffee drying reactor

A fixed, 0.20 m deep shallow bed of parchment coffee modeled via a tensorial form of Fick's second law coupled with energy conservation [56]:

$$\frac{\partial X}{\partial t} = \nabla \cdot (D_m \cdot \nabla X) - r_{evap} \tag{4}$$

$$\frac{\partial (\rho c_p T)}{\partial t} = \nabla \cdot (k_{th} \cdot \nabla T) - \lambda_v \, r_{evap} \tag{5}$$

where D_m is the moisture diffusivity tensor, k_{th} the thermal conductivity tensor, λ_v the latent heat of vaporization, and r_{evap} the volumetric evaporation rate:

$$r_{evap} = k(T,\ a_w)\rho_s \left[X - X_{eq}(T, \phi)\right] \tag{6}$$

with a_w being the local water activity, ϕ ambient relative humidity after desiccant conditioning, and $k(T,\ a_w) = k_0 \exp\left(-\frac{E_a}{RT}\right) f(a_w)$ the apparent drying rate constant [57]. For scoping, silica gel cycle life ~1000 cycles [57], zeolite 13X ~600 cycles [51], capacity fade ~2% per 100 cycles, bed $\Delta p \approx 600$ Pa at design flow, fan power ≈ 80 W, maintenance interval ~6 months for inspection, dust removal, and adsorbent top-up [58].

2.4. Simulation Parameters and Boundary Conditions

Drying air was supplied at a volumetric flow rate [58,59] scaled to dry mass:

$$Q_{\text{air}} = 0.10 \text{ m}^3 \text{ min}^{-1} \text{ kg}^{-1}_{\text{dry coffee}} \tag{7}$$

which yields $Q_{\text{air,tot}} \approx 3.50$ m^3 min^{-1} for $m_{dry} \approx 34$ kg.

Inlet air temperatures T_{in} between 40, 45, and 50 °C were simulated, with inlet relative humidity (post desiccant) between 20 and 50%. The superficial air velocity is computed as $u = Q_{\text{air,tot}}/A$, where $A = 0.50$ m^2. The desiccant bed height was $H_d = 0.15$ m with particle diameter $d_p \approx 3$ mm, porosity $\varepsilon_d = 0.38$, and regeneration performed at 110 °C after each simulated cycle [60]. Convective boundary conditions are applied at the bed–air interface, with heat and mass transfer coefficients (h_T, h_m) obtained from Nusselt and Sherwood correlations in laminar–transitional flow regimes [61].

2.5. Coupling and Driving Force Enhancement

The outlet air from the desiccant bed, with reduced humidity ratio Y_{out}, becomes the inlet air for the drying stage. This modifies the driving force for mass transfer [62] as:

$$\Delta p_{H_2O} = p_{\text{sat}}(T) \cdot a_w - p_{v,\,\infty} \tag{8}$$

where $p_{v,\,\infty}$ is the water vapor partial pressure in the conditioned air stream. Lowering $p_{v,\,\infty}$ increases Δp_{H_2O} without increasing T, thus promoting faster drying as illustrated in Figure 2.

2.6. Energy and Economic Considerations

The desiccant-assisted system shortens drying time by Δt hours relative to a control run without dehumidification. For the reference case, loose coffee husk (Lower Heating Value, LHV ≈ 17 MJ·kg^{-1}) was considered as the representative biofuel commonly used in Colombian coffee farms, allowing a direct assessment of the potential savings in renewable on-farm fuel consumption [49]. The energy required for heating air in the conventional process is:

$$E_{\text{heat}} = \dot{m}_{da} c_{p,\,da} (T_{in} - T_{\text{amb}}) t \tag{9}$$

where $\dot{m}_{da}$ is the dry air mass flow rate and t is the total drying time. The desiccant system reduces t by Δt, yielding proportional savings in thermal energy and biofuel consumption. However, regeneration requires additional energy [63]:

$$E_{\text{regen}} = m_{\text{des}} c_{p,\,\text{des}} \left(T_{\text{regen}} - T_{\text{amb}}\right) + \lambda_v m_{H_2O,\text{ads}} \tag{10}$$

where $m_{H_2O,\text{ads}}$ is the adsorbed water mass to be desorbed. Economic feasibility is assessed by comparing $E_{\text{saved}} - E_{\text{regen}}$ and the associated biofuel cost reductions.

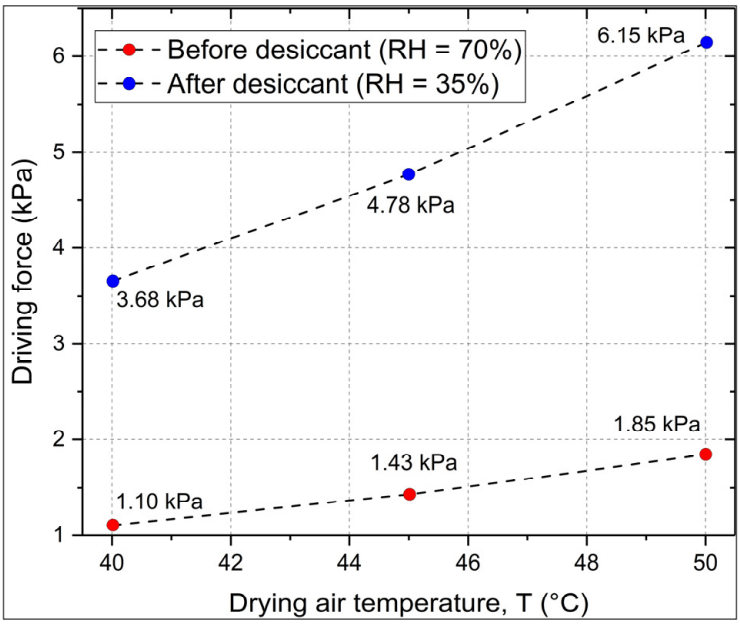

Figure 2. Enhancement of the water vapor driving force (Δp_{H_2O}, expressed as vapor pressure difference in kPa) achieved through desiccant conditioning of inlet air at 40, 45, and 50 °C, for a representative coffee water activity of a_w = 0.85. Comparison shown for pre-desiccant (RH ≈ 70%) and post-desiccant (RH ≈ 35%) conditions.

2.7. Numerical Implementation

The coupled adsorption–drying equations were discretized using a finite-volume scheme with implicit time integration. Equations were discretized via finite-volume scheme with implicit time integration. Tensorial properties D_m and kth were expressed in principal directions of the bed geometry. Convergence criterion:

$$\frac{\left|X^{n+1} - X^n\right|}{X^n} \leq 10^{-6} \tag{11}$$

for all state variables (X, T, Y, q).

All simulations were implemented and solved in MATLAB R2024b (MathWorks, Natick, MA, USA) using custom scripts.

2.8. Reaction Engineering Analogy

The combined coffee–desiccant drying system is formalized within a heterogeneous gas–solid reaction framework, where the adsorption stage functions analogously to a catalytic pre-treatment reactor and the drying stage operates as a reactive porous medium system. The global process can be expressed as a two-step reaction scheme:

I. Adsorption (Catalyst Zone)

$$\text{Air}(Y_{\text{in}}) + \text{Dessicant}\ (q_0) \overset{\text{isothermal}}{\rightarrow} \text{Air}\ (Y_{\text{out}}) + \text{Desiccant}\ (q_{eq}) \tag{12}$$

where Y_{in} and Y_{out} are inlet and outlet humidity rations, and, q_0, q_{eq} are the initial and equilibrium adsorbate loadings on the desiccant. The dynamic adsorption rate is modeled from Equation (3) with:

$$Y_{eq}(T,q) = \frac{p_v}{p_{sat}(T)}\ , \text{ from D} - \text{A isotherm relations (Equation(1))} \tag{13}$$

II. Drying (Reaction Zone)

$$\text{Coffee}(X_0) \overset{T,\phi_{cond},}{\rightarrow}{}^{\Delta pH_2O} \text{Coffee}\left(X_f\right) + H_2O_{(g)} \tag{14}$$

The moisture migration inside the coffee matrix is governed by Equations (4) and (6); however, a sensitivity coefficient was added for each parameter:

$$S_{\theta_i} = \frac{\frac{\partial t_{dry}}{t_{dry}}}{\frac{\partial \theta_i}{\theta_i}} \tag{15}$$

where t_{dry} is the total drying time from X_0 to X_f. Positive $S_{\theta i}$ values indicate prolongation of drying time, whereas negative values represent acceleration.

2.9. Thermodynamic Cycle for Desiccant Regeneration

The regeneration of silica gel type A and zeolite 13X is modeled as a closed-loop thermodynamic cycle comprising adsorption, heating, desorption, and cooling phases. This cycle ensures continuous operation by alternating between adsorption and regeneration beds in a swing configuration. A single-train configuration was assumed, representative of the fixed-bed dryers most commonly used by smallholder farmers, to enable a like-for-like comparison of silica gel and zeolite 13X under identical operating conditions.

The regeneration process is illustrated in Figure 3. Panel A shows the thermodynamic T–s cycle, consisting of four stages: adsorption end (A), heating (B), desorption (C), and cooling (D). Panel B presents the adsorption–desorption isotherm cycle, where the numbered points correspond to adsorption (1–2), saturation (2), desorption (3–4), and regeneration closure (4–1). Together, these diagrams describe both the thermodynamic energy pathway and the sorption equilibrium transitions that govern desiccant cycling.

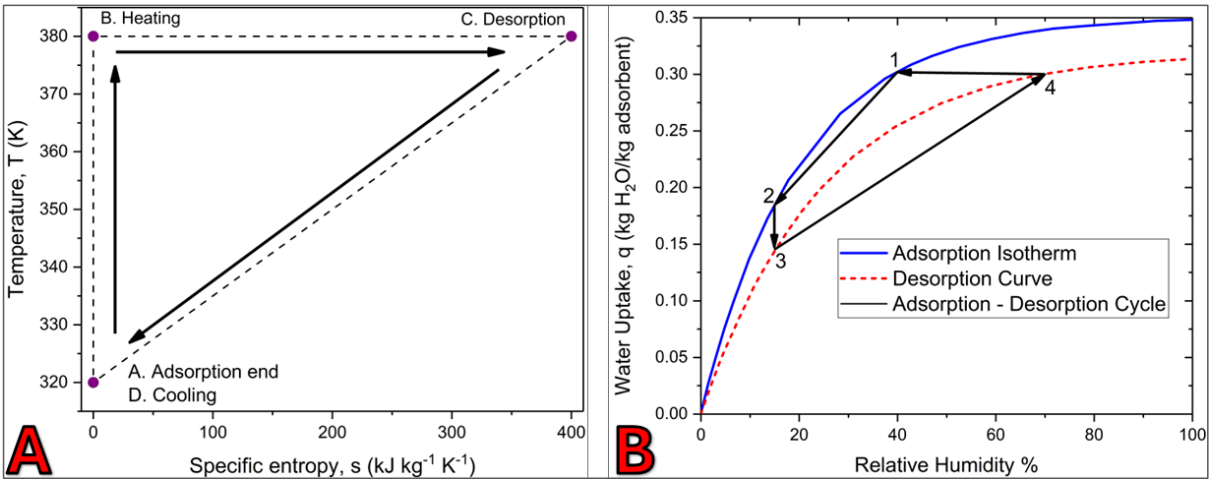

Figure 3. Thermodynamic and sorption cycles for desiccant regeneration. (**A**) T–s diagram with four stages: A. Adsorption end, B. Heating, C. Desorption, D. Cooling. (**B**) Adsorption–desorption isotherm cycle, where numbered points 1–4 correspond to adsorption (1–2), saturation (2), desorption (3–4), and regeneration closure (4–1).

Cycle Stages:

1. Adsorption (A→B):

Isothermal moisture uptake from drying air at T_{ads} (≈ drying inlet temperature). Heat of adsorption, ΔH_{ads}, is released and dissipated via the airflow.

2. Heating (B→C)

The saturated desiccant is heated to regeneration temperature T_{regen} (≈ 110 °C) at constant moisture content. Energy input:

$$Q_{\text{heat}} = m_{\text{des}}\, c_{p,\text{des}}\left(T_{\text{regen}} - T_{\text{amb}}\right) \tag{16}$$

3. Desorption (C→D):

Moisture is driven off at quasi-isothermal T_{regen}, with latent heat requirement:

$$Q_{\text{desorp}} = \lambda_v\, m_{H_2O,\text{ads}} \tag{17}$$

where $m_{H_2O,\text{ads}} = q_{eq} \cdot m_{\text{des}}$.

4. Cooling (D→A):

The regenerated desiccant is cooled back to T_{ads} for re-use. Energy recovery through heat exchange with incoming regeneration air can be implemented for efficiency improvement. The regeneration efficiency is defined as:

$$\eta_{\text{regen}} = \frac{m_{H_2O,\text{ads}}\, \lambda_v}{E_{\text{regen}}} \tag{18}$$

with typical values 0.45–0.65 depending on material.

Total Regeneration Energy Demand:

$$E_{\text{regen}} = Q_{\text{heat}} + Q_{\text{desorp}} \tag{19}$$

Total Regeneration (Saved Energy):

The energy saved by reduced drying time:

$$E_{\text{saved}} = \dot{m}_{\text{da}}\, c_{p,\,\text{da}} (T_{in} - T_{\text{amb}})\, \Delta t \tag{20}$$

Economic feasibility is established if:

$$E_{\text{saved}} - E_{\text{regen}} > 0 \tag{21}$$

This metric is further translated into biofuel mass savings using the specific lower heating value (LHV) of the fuel used for air heating. To simplify the regeneration model, only the sensible heating of the desiccant matrix (Equation (16)) and latent desorption energy (Equation (17)) were included. In practice, additional contributions arise from (i) blower/fan work to circulate purge gas, (ii) sensible and latent loads associated with heating the purge stream, and (iii) inevitable thermal losses through reactor walls and piping as shown in Equation (22).

$$\begin{aligned} \dot{Q}_{\text{heater}} + \dot{W}_{\text{blower}} \quad & + \dot{m}_g c_{p,g}\left(T_{\text{regen}} - T_{in}\right) \\ & = m_{\text{des}} \textstyle\int_{T_{\text{amb}}}^{T_{\text{regen}}} c_{p,\text{des}}(T)\, dT + m_{H_2O,\text{ads}}\, \lambda_v\left(T_{\text{regen}}\right) + \dot{Q}_{\text{loss}} \end{aligned} \tag{22}$$

where $\dot{Q}_{\text{heater}}$ is the heater duty, $\dot{W}_{\text{blower}}$ the blower/fan work, $\dot{m}_g$ the purge-gas mass flow rate, and $c_{p,g}$ its heat capacity. On the right-hand side, m_{des} is the desiccant mass, $c_{p,\text{des}}$

(T) its specific heat capacity, $m_{H_2O,\text{ads}}$ the mass of desorbed water, λ_v (T_{regen}) the latent heat of vaporization, and $\dot{Q}_{\text{loss}}$ the thermal losses. In the present work, this balance was simplified by treating $c_{p,\text{des}}$ and λ_v as constants and neglecting blower work, purge-gas loads, and heat losses. These terms should be included in detailed experimental or techno-economic studies since these factors can raise the effective regeneration demand by 10–20% depending on design and insulation quality [39].

3. Results and Discussion

3.1. Drying Kinetics Under Desiccant-Assisted and Control Conditions

Simulated drying curves of parchment coffee, expressed as dimensionless moisture ratio X/X_0 versus time, are shown in Figure 4. In the control scenario, where drying air was conditioned solely by heating, the total drying time to reach the target final moisture content (X_f = 10–12% (wb)) was approximately 40 h at 40 °C, 30 h at 45 °C, and 23 h at 50 °C. These values are consistent with experimental data for low-temperature thin-bed drying of coffee parchment reported in previous studies [2,10,42]. Drying curves were derived from a Fickian diffusion basis with effective diffusivity, embedded in the tensorial transport equations, rather than from empirical thin-layer models such as Page or Henderson–Pabis [64,65].

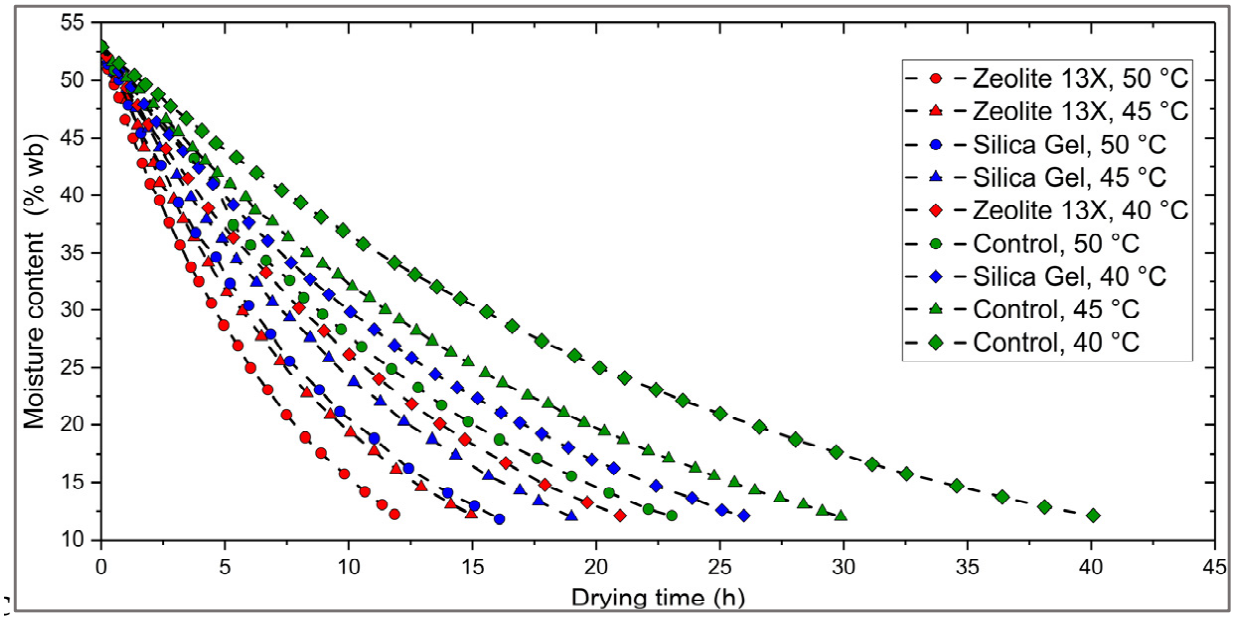

Figure 4. Simulated drying curves of parchment coffee under control (heated air) and desiccant-assisted (silica gel and zeolite 13X) conditions at 40, 45, and 50 °C. Initial moisture was 53% (wb) with a target of 10–12% (wb). Desiccant-assisted runs show markedly steeper slopes and shorter drying times compared to control.

The introduction of desiccants produced a marked acceleration of drying. At 40 °C, silica gel reduced drying time from 40 h to 26 h (35% reduction), while zeolite 13X further shortened it to 21 h (47% reduction). At 45 °C, silica gel required only 19 h and zeolite 15 h, compared to 30 h for the control. At 50 °C, silica gel reduced the drying cycle from 23 h to 15 h, whereas zeolite reached the endpoint in 12 h, translating into reductions of ~35% and ~46%, respectively. The quantitative comparison is summarized in Table 1, which also reports the apparent drying constants (k) fitted from the falling-rate period.

Table 1. Drying times and apparent drying constants (k) of parchment coffee under different inlet air temperatures with and without desiccant assistance.

Inlet Air Temp (°C)	Control		Silica Gel			Zeolite 13X		
	Time (h)	k (h^{-1})	Time (h)	Reduction (%)	k (h^{-1})	Time (h)	Reduction (%)	k (h^{-1})
40	40	0.032	26	35%	0.048	21	47%	0.056
45	30	0.041	19	36.7%	0.062	15	50%	0.071
50	23	0.050	15	34.8%	0.073	12	46%	0.082

These curves highlight the role of the desiccant in enhancing the psychrometric driving force. By lowering the absolute humidity of the drying air, the effective vapor pressure gradient between the coffee matrix and the surrounding air increased, leading to faster moisture migration [66–68]. The effect was most pronounced during the falling-rate period, where diffusion and desorption resistances typically dominate [69,70]. Notably, the desiccant-assisted process maintained steeper drying curves even at lower air temperatures, indicating that desiccants can partially substitute for thermal input by providing an alternative pathway to intensification [71].

From an engineering perspective, increasing inlet air temperature by 5 °C in the control runs reduced drying time by ~25–30%. However, the addition of desiccants under identical conditions provided an additional 30–40% reduction, underscoring their potential as a complementary rather than competing approach to heat input [72]. This synergy demonstrates that energy demand can be moderated without sacrificing throughput, which is especially relevant in smallholder contexts where fuel availability or electrical supply may be constrained [73,74].

Figure 4 clearly illustrates these differences, showing that zeolite consistently outperforms silica gel, though both materials deliver significant benefits compared to the control. The early divergence of the desiccant-assisted curves indicates faster transition through the constant-rate period, while the steeper slope during the falling-rate stage confirms sustained drying acceleration throughout the process [75,76].

3.2. Comparative Performance of Silica Gel and Zeolite 13X

A direct comparison between silica gel and zeolite 13X reveals significant differences in adsorption capacity, kinetics, and the resulting impact on drying behavior. Silica gel, with a relatively high uptake at moderate humidity levels, provided effective acceleration of drying, particularly at 40 °C where it reduced drying time by approximately 14 h compared to the control (Table 1). However, zeolite 13X consistently outperformed silica gel across all operating temperatures, owing to its stronger affinity for water and steeper isotherm slope in the low relative humidity region [77,78]. At 40 °C, zeolite shortened drying by 19 h relative to the control, surpassing silica gel by an additional 5 h. At 50 °C, the difference widened further, with zeolite achieving final moisture content in 12 h versus 15 h for silica gel.

The superior performance of zeolite is further evidenced in Figure 5, which presents outlet humidity ratio (Y_{out}) as a function of drying time at 40, 45, and 50 °C. In the control case, Y_{out} quickly approached saturation values of ~0.014 kg $H_2O \cdot kg^{-1}$ dry air, causing the psychrometric driving force to collapse. Silica gel maintained lower humidity ratios (~0.008) for longer durations, sustaining moisture removal during the falling-rate period. Zeolite 13X consistently achieved the lowest plateaus (~0.006), and its Y_{out} profile remained well below both the control and silica gel throughout the process. This air-side perspective explains why zeolite enabled steeper drying curves in Figure 4 and more efficient use of

adsorbent mass: the desiccant delayed breakthrough and preserved a strong vapor pressure gradient across the entire cycle.

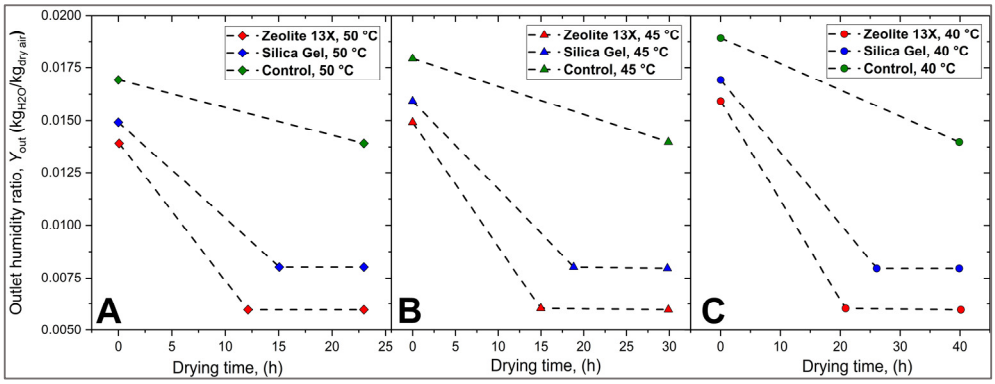

Figure 5. Outlet humidity ratio (Y_{out}) versus drying time at 40 °C (**C**), 45 °C (**B**), and 50 °C (**A**) for control air, silica gel, and zeolite 13X. Zeolite maintained the lowest Y_{out} plateaus, sustaining stronger psychrometric driving forces throughout drying.

From a practical standpoint, silica gel remains attractive due to its lower cost, widespread availability, and relatively mild regeneration requirements (~110 °C). Zeolite, however, combines superior adsorption efficiency with higher regeneration energy demand (~250–300 °C), raising economic trade-offs that must be considered in farm-level applications. Thus, while zeolite 13X demonstrates clear technical superiority in sustaining lower humidity ratios and faster kinetics, silica gel may present a more feasible option in contexts where energy resources for regeneration are limited.

Table 2 summarizes the comparative performance parameters of silica gel and zeolite 13X. While zeolite maintains lower outlet humidity ratios for longer durations and delivers up to 50 times reduction, it requires higher loading per batch and more energy-intensive regeneration. Silica gel, by contrast, provides moderate but still substantial drying enhancement under milder regeneration conditions, aligning better with farm-level energy availability [31].

Table 2. Comparative parameters of silica gel type A and zeolite 13X for desiccant-assisted coffee drying.

Parameter	Silica Gel A	Zeolite 13X
Typical loading per 70 kg batch [1]	26–44 kg	36–59 kg
Breakthrough time [2]	6–8 h	9–12 h
Minimum outlet humidity ratio ($Y_{out,min}$) [3]	~0.008 kg $H_2O \cdot kg^{-1}$ dry air	~0.006 kg $H_2O \cdot kg^{-1}$ dry air
Relative drying time reduction [4]	35–37%	46–50%
Regeneration temperature [3]	~110–130 °C	~250–300 °C
Regeneration energy demand	Low–moderate	High
Material cost (relative)	Low	Moderate–high

[1] Based on simulation at 40–50 °C, airflow = 0.1 $m^3 \cdot min^{-1} \cdot kg^{-1}$ dry coffee.[2] Time until outlet RH begins to approach inlet RH, indicating loss of adsorption efficiency.[3] Based on the [51,52,78–80] findings.[4] Relative to control heated-air drying at same temperature.

3.3. Energy Balance, Regeneration Cost, and Feasibility Window

The integration of desiccants into the drying process modifies the overall energy balance by simultaneously reducing the thermal demand for air heating and introducing

the additional cost of desiccant regeneration. In the control scenario, the total energy requirement is dominated by the enthalpy input needed to heat the drying air stream from ambient (T_{amb}) to the selected inlet temperature (T_{in}), sustained over the full drying duration ($t_{control}$) as seen in Equation (9), where $\dot{m}_{\mathrm{da}}$ is the mass flow rate of dry air and $c_{p,da}$ its specific heat capacity.

When a desiccant bed is integrated, the drying time is reduced by Δt, leading to proportional savings in heating energy as stated in Equation (20). At 45 °C, silica gel shortened drying by ~11 h, while zeolite 13X achieved ~15 h reduction (Table 1), corresponding to heating energy savings of 30–40% compared to the control. This reduction is significant because fuel consumption scales linearly with time in forced-convection dryers; thus, every additional hour saved translates into measurable fuel savings and lower operating costs.

The trade-off arises from desiccant regeneration. Silica gel requires only moderate temperatures (110–130 °C) to restore capacity, allowing regeneration to be achieved using low-grade heat sources such as biomass combustion gases, solar thermal collectors, or waste heat streams. Zeolite 13X, by contrast, demands considerably higher regeneration temperatures (250–300 °C) to overcome stronger binding energies, making it more energy-intensive to cycle. The regeneration load can be expressed as stated in Equation (10).

For the simulated 70 kg coffee batch, this represented ~26–44 kg of silica gel and ~36–59 kg of zeolite per run (Table 2). It is important to emphasize that, while the regeneration sequence is conceptually the same for both desiccants, their thermal demands are quite different. Silica gel requires only 110–130 °C and can be regenerated with simple rigs using biomass flue gas or solar heat, whereas zeolite 13X demands 250–300 °C, requiring more robust heating systems or renewable/waste heat integration. This distinction underscores that silica gel is better suited for smallholder conditions, while zeolite may be viable only where higher-grade energy inputs are available.

The net balance between energy saved during drying and energy required for regeneration defines the feasibility window of desiccant-assisted systems. As shown in Figure 6, both silica gel and zeolite remain feasible since their net energy balances are positive across all tested temperatures. Silica gel provided the most robust margin, with net savings of ~17–25%, while zeolite achieved only ~6–12%. This difference highlights that while zeolite accelerates drying more strongly, the advantage is partially offset by its more expensive regeneration.

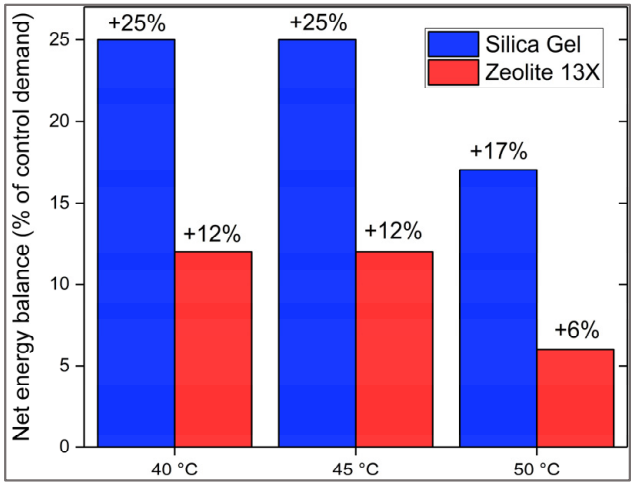

Figure 6. Net energy balance of desiccant-assisted drying relative to control at 40, 45, and 50 °C. Positive values indicate that energy savings from shorter drying times exceeded the energy required for desiccant regeneration.

From an economic perspective, the value of reduced drying times becomes evident when expressed in terms of renewable biofuel use, these savings correspond to a reduction of approximately 1.6–1.8 kg of loose coffee husks per batch with silica gel, directly lowering the fuel-demand. With loose coffee husk (LHV $\approx$ 17 MJ·kg^{-1}, ~0.05 USD·kg^{-1}), the control run at 45 °C required ~5.2 kg of fuel (~0.26 USD). Silica gel reduced this by 1.6–1.8 kg (~0.08–0.09 USD), while zeolite achieved only ~0.02–0.04 USD net savings. When fossil fuels are considered, the cost differentials widen. Diesel (LHV $\approx$ 43 MJ·kg^{-1}, ~1.10 USD·L^{-1}) and Liquefied Petroleum Gas (LPG) (46 MJ·kg^{-1}, ~0.90 USD·kg^{-1}) translate the energy savings of silica gel into ~0.40–0.50 USD per batch, while zeolite remains marginal unless heat recovery or renewable regeneration sources are employed, also, considering commercial costs, silica gel ($\approx$ 2–3 USD·kg^{-1}) remains more economically favorable than zeolite 13X ($\approx$ 4–6 USD·kg^{-1}), as its lower market price aligns with its reduced regeneration demand, further strengthening its feasibility at farm scale [36]. These values are summarized in Table 3.

Table 3. Estimated fuel consumption and cost savings per 70 kg batch of wet coffee dried at 45 °C under control and desiccant-assisted conditions. Columns show both fuel use (kg or L) and corresponding costs (USD). Values are based on reference fuel prices (husk by mass, diesel by volume, LPG by mass), assuming an average burner efficiency of 70% and constant local market prices; no density corrections or variability effects are included.

Fuel Source	Control (Fuel, Cost)	Silica Gel Savings (Fuel, Cost)	Silica Gel Net Cost	Zeolite Savings (Fuel, Cost)	Zeolite Net Cost
Coffee husk (LHV 17 MJ·kg^{-1}, 0.05 USD·kg^{-1})	5.2 kg (0.26 USD)	1.6–1.8 kg (0.08–0.09 USD)	0.17–0.18 USD	0.5–0.8 kg (0.02–0.04 USD)	0.22–0.24 USD
Diesel (LHV 43 MJ·kg^{-1}, 1.10 USD·L^{-1})	0.65 L (0.72 USD)	0.20–0.25 L (0.22–0.27 USD)	0.45–0.50 USD	0.06–0.10 L (0.07–0.11 USD)	0.61–0.65 USD
LPG (LHV 46 MJ·kg^{-1}, 0.90 USD·kg^{-1})	0.63 kg (0.57 USD)	0.19–0.24 kg (0.17–0.22 USD)	0.35–0.40 USD	0.06–0.10 kg (0.05–0.09 USD)	0.52–0.55 USD

Although the absolute savings appear modest on a per-batch basis, the cumulative effect across a harvest season is non-trivial. For a smallholder drying ~100 batches per year, silica gel integration translates into 8–10 USD savings with husk fuel, but up to 40–50 USD if fossil fuels are used. At a cooperative or community dryer handling hundreds of batches, these savings scale substantially [81]. More importantly, shorter drying times increase processing capacity and reduce the risk of bottlenecks or microbial spoilage during peak harvests, which represents an indirect but crucial economic benefit not captured in fuel costs alone [82]. For comparability, fuel costs were normalized to delivered useful heat as $C_{\text{useful}} = \frac{\text{price}}{(\text{LHV}\ \eta)}$, using η = 0.70, reference values are $\approx$ 4.2 USD·GJ^{-1} (husk, 17 MJ·kg^{-1}), $\approx$ 28 USD·GJ^{-1} (LPG, 46 MJ·kg^{-1}), and $\approx$ 44 USD·GJ^{-1} (diesel, $\approx$ 36 MJ·L^{-1} from 43 MJ·kg^{-1} and $\rho \approx 0.84$ kg·L^{-1}). A one-way sensitivity with $\eta \in [0.60, 0.80]$ and $\pm$25% price variation yields ranges of 3.7–4.9 (husk), 24–33 (LPG), and 38–51 (diesel) USD·GJ^{-1}; the relative ranking is unchanged.

Figure 6 consequently illustrates the dual perspective: both desiccants are energetically feasible, but silica gel provides a consistently stronger balance between drying acceleration and regeneration cost. Zeolite offers superior kinetics but narrower economic viability unless regeneration energy can be sourced cheaply or sustainably. In addition, long-term feasibility depends on desiccant durability, attrition, and the cost of repeated regeneration cycles. While silica gel and zeolite are both regenerable, material losses can occur due to handling and cycling stress, and adsorbent replacement may be required after extended use. Durability testing under farm-level conditions will be necessary to determine the effective lifetime of desiccants, their resistance to attrition, and the practical frequency of

regeneration. These factors introduce additional costs beyond single-batch savings and should be incorporated into future techno-economic analyses.

3.4. Sensitivity Analysis and Scaling Guidelines

The performance of desiccant-assisted drying depends strongly on operating conditions. Sensitivity analysis was carried out to assess the relative impact of air temperature, ambient humidity, airflow rate, and desiccant loading, allowing identification of the conditions where desiccants provide the greatest benefit.

Temperature sensitivity. Increasing inlet air temperature accelerated drying in both control and desiccant-assisted cases, but the relative benefit of desiccants was greatest at lower temperatures. At 40 °C, silica gel and zeolite reduced drying times by 35–47% compared to control, whereas at 50 °C the reductions were ~32–46%. This reflects the fact that heating alone already creates a strong vapor pressure gradient at higher T, so the marginal benefit of dehumidification decreases [26,80]. Practically, this implies that desiccant integration is most valuable in low to mid-temperature regimes (35–45 °C), which are often preferred for coffee to preserve sensory quality and seed viability [82,83].

Relative humidity (RH). Ambient RH proved to be the most critical factor. Under humid-season conditions (RH $\geq$ 80%), desiccant assistance nearly halved drying time relative to the control, whereas under drier conditions (RH 50–60%) the advantage shrank to ~15–20% [35]. The results confirm that desiccants are especially useful in equatorial coffee zones where harvest coincides with rainy periods [84,85]. In such contexts, desiccants not only reduce fuel consumption but also mitigate the risks related to incomplete drying [86].

Airflow rate. Convective transfer interacts strongly with desiccant efficiency. At low velocities (<0.05 $m \cdot s^{-1}$), external film resistance limited the drying rate, so the benefit of lowering air humidity was not fully exploited [59]. At intermediate flows (0.10–0.15 $m \cdot s^{-1}$), the synergy between high mass transfer coefficients and drier air yielded kinetic promotion factors up to 2.3 times more compared to control [54]. However, airflow increases also raise fan energy demand and may incur higher operating costs [87]. This highlights the need to optimize fan sizing relative to desiccant loading, rather than maximizing one parameter in isolation.

Desiccant loading. Bed mass also exhibited a threshold effect. Undersized beds saturated within 4–5 h, causing outlet humidity ratios to rise and eroding the initial advantage [88,89]. On the other hand, oversizing above ~40 kg silica or ~55 kg zeolite per 70 kg coffee batch provided only marginal improvements in drying time but substantially increased regeneration demand [90]. Hence, the most efficient operating point balances breakthrough time with regeneration feasibility, reinforcing the analogy with optimal catalyst loading in chemical reactors [36,90].

To support practical design, a scaling guideline is proposed in Figure 7, showing desiccant mass requirements as a function of airflow rate and target humidity ratio reduction (ΔY). The chart indicates, for instance, that achieving ΔY = 0.006 kg $H_2O \cdot kg^{-1}$ at 0.10 $m^3\ min^{-1} \cdot kg^{-1}$ dry coffee requires ~34 kg silica gel or ~48 kg zeolite. Such nomographs can be used to adapt the technology to diverse farm scales: at smallholder level, prioritizing minimal desiccant mass to reduce regeneration energy; at cooperative dryers, integrating larger beds with heat recovery systems to exploit zeolite's superior kinetics [91]. Figure 7 should be read with practical constraints: footprint-limited bed thickness $\leq$ 0.20 m, superficial velocity 0.06–0.10 m s^{-1}, allowable pressure drop $\leq$800 Pa, and available desiccant mass and heater capacity; selections outside these bounds imply higher capital, fan power, or floor area.

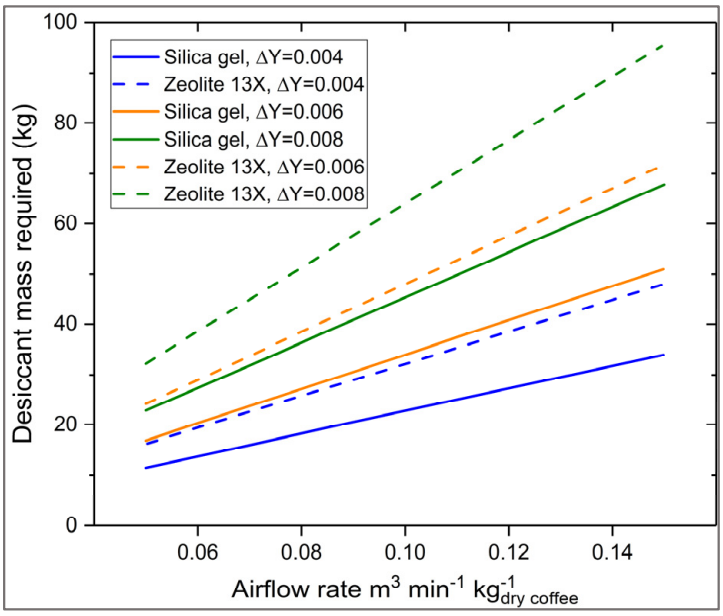

Figure 7. Nomograph of desiccant mass requirements as a function of airflow rate and target humidity ratio reduction (ΔY) for silica gel (solid lines) and zeolite 13X (dashed lines). Nomograph use is subject to footprint, Δp, and capacity limits noted in Section 3.4.

Overall, the sensitivity analysis confirms that desiccant-assisted drying is most advantageous under humid, low- to mid-temperature conditions with moderate airflow and optimally sized beds [26,39,89]. The scaling guidelines bridge modeling results with field application, enabling rational adaptation of the system across contexts ranging from household-level solar dryers to large mechanical units [90,91].

4. Conclusions

This work introduced a novel approach to postharvest coffee drying, reconceptualized as a gas–solid dehydration process enhanced by regenerable desiccants acting as catalyst analogs. By lowering the humidity ratio of the drying air, desiccants intensified the psychrometric driving force and accelerated moisture removal. Simulations showed that at 40–50 °C, silica gel reduced drying times by 35–37%, while zeolite 13X achieved 46–50% reductions, reflecting its stronger adsorption capacity and sustained outlet humidity control.

Energetic evaluation demonstrated that both materials are feasible, since the energy savings from shorter drying cycles exceeded regeneration costs. Silica gel provided the most favorable balance, with net savings of 17–25% owing to its low regeneration temperature (110–130 °C). Zeolite 13X delivered superior kinetics but achieved only 6–12% net savings because of its higher regeneration temperature (250–300 °C), making it most attractive when low-cost or renewable heat sources are available. Economic analysis confirmed that silica gel consistently translates into meaningful per-batch fuel savings under both biofuel and fossil fuel scenarios, while zeolite requires careful consideration of regeneration energy supply.

Scalability was addressed through sensitivity analysis and a nomograph of desiccant mass versus airflow and humidity targets. These results indicate that desiccant-assisted drying is most advantageous under humid-season conditions, at moderate temperatures, and with properly dimensioned beds. Importantly, the framework demonstrates that desiccant-assisted drying enhances efficiency when using renewable biofuels such as loose coffee husks, reinforcing its sustainability and practical relevance for smallholder systems in humid tropical regions.

Although this study was based on simulation, it establishes a rigorous proof-of-concept bridging chemical reaction engineering with coffee drying. In addition to the modeling results presented here, future research should experimentally validate desiccant-assisted coffee drying at pilot and farm scales, assessing drying kinetics, adsorbent stability across multiple cycles, and practical regeneration strategies, to translate this theoretical framework into field-ready applications. Experimental determination of heat and mass transport parameters in parchment coffee is also needed, as microstructural variability can significantly influence drying kinetics and should be integrated to refine and validate the model. Such validation will extend the merit of this work, consolidating its potential as a practical and scalable solution for coffee producers in humid tropical regions worldwide.

Funding: This research was funded by the European Union's Horizon EUSPA-2022-SPACE research and innovation actions under grant agreement No. 101131859 (COMUNIDAD).

Data Availability Statement: The raw data supporting the conclusions of this article will be made available by the author on request.

Acknowledgments: The author gratefully acknowledges the National Coffee Research Centre of Colombia (Cenicafé) for institutional support and the Discipline of Postharvest for their technical and scientific contributions during the development of this work.

Conflicts of Interest: The author declares no conflicts of interest.

References

1. Worku, M.; Astatkie, T.; Boeckx, P. Effect of Growing Conditions and Postharvest Processing on Arabica Coffee Bean Physical Quality Features and Defects. *Heliyon* **2022**, *8*, e09201. [CrossRef] [PubMed]
2. Borém, F.M.; Andrade, E.T. de Processing and Drying of Coffee. In *Drying and Roasting of Cocoa and Coffee*; CRC Press: Boca Raton, FL, USA, 2019; ISBN 978-1-315-11310-4.
3. Poltronieri, P.; Rossi, F. Challenges in Specialty Coffee Processing and Quality Assurance. *Challenges* **2016**, *7*, 19. [CrossRef]
4. Restrepo Salazar, I.C.; Peñuela Mesa, G.A. Influence of Temperature, Relative Humidity, and Storage Time Conditions on Ochratoxin a Production by Aspergillus Niger Fungi in Dry Parchment Coffee. *Food Addit. Contam. Part A* **2025**, *42*, 491–502. [CrossRef]
5. Paterson, R.R.M.; Lima, N.; Taniwaki, M.H. Coffee, Mycotoxins and Climate Change. *Food Res. Int.* **2014**, *61*, 1–15. [CrossRef]
6. Adhikari, M.; Isaac, E.L.; Paterson, R.R.M.; Maslin, M.A. A Review of Potential Impacts of Climate Change on Coffee Cultivation and Mycotoxigenic Fungi. *Microorganisms* **2020**, *8*, 1625. [CrossRef]
7. Wang, X.; Wang, Y.; Hu, G.; Hong, D.; Guo, T.; Li, J.; Li, Z.; Qiu, M. Review on Factors Affecting Coffee Volatiles: From Seed to Cup. *J. Sci. Food Agric.* **2022**, *102*, 1341–1352. [CrossRef]
8. Dong, W.; Hu, R.; Chu, Z.; Zhao, J.; Tan, L. Effect of Different Drying Techniques on Bioactive Components, Fatty Acid Composition, and Volatile Profile of Robusta Coffee Beans. *Food Chem.* **2017**, *234*, 121–130. [CrossRef]
9. Kulapichitr, F.; Borompichaichartkul, C.; Suppavorasatit, I.; Cadwallader, K.R. Impact of Drying Process on Chemical Composition and Key Aroma Components of Arabica Coffee. *Food Chem.* **2019**, *291*, 49–58. [CrossRef]
10. Duque-Dussán, E.; Sanz-Uribe, J.R.; Banout, J. Design and Evaluation of a Hybrid Solar Dryer for Postharvesting Processing of Parchment Coffee. *Renew. Energy* **2023**, *215*, 118961. [CrossRef]
11. Duque-Dussán, E.; Ramírez-Gómez, C.A.; Guerrero-Aguirre, Á.; Rojas-Botina, W.F.; Sanz-Uribe, J.R. Evaluation of Modular Polycarbonate Solar Dryers for Coffee: Technical Performance and Economic Feasibility. *J. Food Process Eng.* **2025**, *48*, e70165. [CrossRef]
12. de Sousa e Silva, J.; Moreli, A.P.; Donzeles, S.M.L.; Soares, S.F.; Vitor, D.G. Harvesting, Drying and Storage of Coffee. In *Quality Determinants in Coffee Production*; Louzada Pereira, L., Rizzo Moreira, T., Eds.; Springer International Publishing: Cham, Switzerland, 2021; pp. 1–6, ISBN 978-3-030-54437-9.
13. Meja, E.M.; Dubbe, S.K.; Bekele, A.; Wolde, K.F.; Adaramola, M.S. Investigating the Performance and Optimization of Solar Coffee Drying Technologies—A Systematic Review. *J. Food Process. Preserv.* **2025**, *2025*, 7907660. [CrossRef]
14. Zziwa, A.; Sempiira, J.E.; Kizito, S.S.; Kabenge, I.; Soddo, P. Accelerating Coffee Drying with Innovation: Performance Evaluation of a Sensor-Controlled Hybrid Solar-Biomass Powered Dryer for Coffee Drying in Uganda. *Sustain. Energy Technol. Assess.* **2025**, *82*, 104507. [CrossRef]

15. Manrique, R.; Vásquez, D.; Chejne, F.; Pinzón, A. Energy Analysis of a Proposed Hybrid Solar–Biomass Coffee Bean Drying System. *Energy* **2020**, *202*, 117720. [CrossRef]
16. da Costa, F.O.; Alvarenga, T.F.; de Mesquita, T.V.C.; Petri Júnior, I. Hybrid Drying of Pulped Arabica Coffee Cherry Beans (*Coffea arabica* L. Cv. Catuai) Using a Hexagonal Microwave Dryer Designed by Numerical Simulations. *J. Food Process Eng.* **2021**, *44*, e13666. [CrossRef]
17. Chen, W.-H.; Chen, G.-H.; Lee, K.-T.; Gunarathne, D.S.; Hoang, A.T. Synergetic Strategy: Upgrading Fuel Properties of Waste Starch Composite Fuels by Blending Torrefied Spent Coffee Grounds. *J. Taiwan Inst. Chem. Eng.* **2024**, 105820. [CrossRef]
18. Rocha, T.d.A.F.; Ferreira, M.D.C.; Freire, J.T. Processing Spent Coffee Ground Powders for Renewable Energy Generation: Mechanical Dewatering and Thermal Drying. *Process Saf. Environ. Prot.* **2021**, *146*, 300–311. [CrossRef]
19. Lee, K.-T.; Tsai, J.-Y.; Hoang, A.T.; Chen, W.-H.; Gunarathne, D.S.; Tran, K.-Q.; Selvarajoo, A.; Goodarzi, V. Energy-Saving Drying Strategy of Spent Coffee Grounds for Co-Firing Fuel by Adding Biochar for Carbon Sequestration to Approach Net Zero. *Fuel* **2022**, *326*, 124984. [CrossRef]
20. Villagran, E.; Espitia, J.J.; Velázquez, F.A.; Rodriguez, J. Solar Dryers: Technical Insights and Bibliometric Trends in Energy Technologies. *AgriEngineering* **2024**, *6*, 4041–4063. [CrossRef]
21. John, M.K.; Bandaru, R.; Zachariah, T.J. Comparative Review with a Field Survey on Conventional and Advanced Solar Dryers in Agricultural Processing. *J. Therm. Anal. Calorim.* **2025**, *150*, 10267–10298. [CrossRef]
22. Nilnont, W.; Thepa, S.; Janjai, S.; Kasayapanand, N.; Thamrongmas, C.; Bala, B.K. Finite Element Simulation for Coffee (*Coffea arabica*) Drying. *Food Bioprod. Process.* **2012**, *90*, 341–350. [CrossRef]
23. Oliveros, N.O.; Hernández, J.A.; Sierra-Espinosa, F.Z.; Guardián-Tapia, R.; Pliego-Solórzano, R. Experimental Study of Dynamic Porosity and Its Effects on Simulation of the Coffee Beans Roasting. *J. Food Eng.* **2017**, *199*, 100–112. [CrossRef]
24. Burmester, K.; Fehr, H.; Eggers, R. A Comprehensive Study on Thermophysical Material Properties for an Innovative Coffee Drying Process. *Dry. Technol.* **2011**, *29*, 1562–1570. [CrossRef]
25. Abdelgaied, M.; Saber, M.A.; Bassuoni, M.M.; Khaira, A.M. Adsorption Air Conditioning: A Comprehensive Review in Desiccant Materials, System Progress, and Recent Studies on Different Configurations of Hybrid Solid Desiccant Air Conditioning Systems. *Envron. Sci. Pollut. Res.* **2023**, *30*, 28344–28372. [CrossRef]
26. Djaeni, M.; A'yuni, D.Q.; Alhanif, M.; Hii, C.L.; Kumoro, A.C. Air Dehumidification with Advance Adsorptive Materials for Food Drying: A Critical Assessment for Future Prospective. *Dry. Technol.* **2021**, *39*, 1648–1666. [CrossRef]
27. Kumar, S.; Salins, S.S.; Kuroor, U.K.; D'Souza, S.W.; Bose, A. Impact of Dry Rice Grain Packing Density and Time on the Performance of Two Stage Dehumidifier. *Sci. Rep.* **2025**, *15*, 16908. [CrossRef]
28. Chai, S.; Kong, X.; Mercangöz, M. State Estimation for Industrial Desiccant Air Dryers Using Hybrid Mechanistic and Machine Learning Models. *Comput. Ind.* **2025**, *168*, 104274. [CrossRef]
29. Jeong, Y.; Ansari, J.R.; Sadeghi, K.; Seo, J. Applicability of Polypropylene/Polyethylene Glycol/Molecular Sieve Composites as Desiccant Pharmaceutical Packaging Materials. *Food Packag. Shelf Life* **2024**, *42*, 101266. [CrossRef]
30. Anokye-Bempah, L.; Han, J.; Kornbluth, K.; Ristenpart, W.; Donis-González, I.R. The Use of Desiccants for Proper Moisture Preservation in Green Coffee during Storage and Transportation. *J. Agric. Food Res.* **2023**, *11*, 100478. [CrossRef]
31. Sanjay; Mishra, S.; Alam, T. Experimental Investigation on Storage of Food Grains Using Cow Dung-Based Desiccant as Preservative. *Energy Sources Part A Recovery Util. Environ. Eff.* **2023**, *45*, 12018–12039. [CrossRef]
32. Zeeshan, M.; Tufail, I.; Khan, S.; Khan, I.; Ayuob, S.; Mohamed, A.; Chauhdary, S.T. Novel Design and Performance Evaluation of an Indirectly Forced Convection Desiccant Integrated Solar Dryer for Drying Tomatoes in Pakistan. *Heliyon* **2024**, *10*, e29284. [CrossRef]
33. Fadiji, T.; Rashvand, M.; Daramola, M.O.; Iwarere, S.A. A Review on Antimicrobial Packaging for Extending the Shelf Life of Food. *Processes* **2023**, *11*, 590. [CrossRef]
34. Meshcheryakov, E.P.; Reshetnikov, S.I.; Sandu, M.P.; Knyazev, A.S.; Kurzina, I.A. Efficient Adsorbent-Desiccant Based on Aluminium Oxide. *Appl. Sci.* **2021**, *11*, 2457. [CrossRef]
35. Mittal, H.; Al Alili, A.; Alhassan, S.M.; Agung Susantyoko, R. Zeolites and Superporous Hydrogels-Based Hybrid Composites as Solid Desiccants to Capture Water Vapors from Humid Air. *Microporous Mesoporous Mater.* **2022**, *342*, 112116. [CrossRef]
36. Hraiech, I.; Zallama, B.; Belkhiria, S.; Zili-Ghedira, L.; Maatki, C.; Hassen, W.; Hadrich, B.; Kolsi, L. Experimental Characterization of Silica Gel Adsorption and Desorption Isotherms under Varying Temperature and Relative Humidity in a Fixed Bed Reactor. *Sci. Rep.* **2025**, *15*, 29041. [CrossRef]
37. Majumder, P.; Sinha, A.; Gupta, R.; Sablani, S.S. Drying of Selected Major Spices: Characteristics and Influencing Parameters, Drying Technologies, Quality Retention and Energy Saving, and Mathematical Models. *Food Bioprocess. Technol.* **2021**, *14*, 1028–1054. [CrossRef]
38. Hua, L.; Wang, R. An Exergy Analysis and Parameter Optimization of Solid Desiccant Heat Pumps Recovering the Condensation Heat for Desiccant Regeneration and Heat Transfer Enhancement. *Energy* **2022**, *238*, 121811. [CrossRef]

39. Gorai, V.K.; Singh, S.K.; Jani, D.B. A Comprehensive Review on Solid Desiccant-Assisted Novel Dehumidification and Its Advanced Regeneration Methods. *J. Therm. Anal. Calorim.* **2024**, *149*, 8979–9000. [CrossRef]
40. Zeng, Y.; Woods, J.; Cui, S. The Energy Saving Potential of Thermo-Responsive Desiccants for Air Dehumidification. *Energy Convers. Manag.* **2021**, *244*, 114520. [CrossRef]
41. Andrade, P.S.; Duarte, C.R.; Barrozo, M.A.S. An Innovative Dryer for Arabica Coffee (*Coffea arabica* L.) Drying: Investigating Heat and Mass Transfer. *Dry. Technol.* **2024**, *42*, 1065–1076. [CrossRef]
42. Collazos-Escobar, G.A.; Gutiérrez-Guzmán, N.; Váquiro, H.A.; García-Pérez, J.V.; Cárcel, J.A. Analysis of Machine Learning Algorithms for the Computer Simulation of Moisture Sorption Isotherms of Coffee Beans. *Food Bioprocess. Technol.* **2025**, *18*, 5419–5430. [CrossRef]
43. Zhu, Z.; Zhang, M. Water Vapor Adsorption on Desiccant Materials for Rotary Desiccant Air Conditioning Systems. *Processes* **2023**, *11*, 2166. [CrossRef]
44. Almasarani, A.; Ahmad, I.K.; El-Amin, M.F.; Brahimi, T. Experimental Investigations and Modeling of Atmospheric Water Generation Using a Desiccant Material. *Energies* **2022**, *15*, 6834. [CrossRef]
45. *ICC-122-12-e*; National Quality Standards. International Coffee Organization (ICO): London, UK, 2018.
46. Montilla-Pérez, J.; Arcila-Pulgarín, J.; Aristizábal-Loaiza, M.; Montoya-Restrepo, E.C.; Puerta-Quintero, G.I.; Oliveros-Tascón, C.E.; Cadena-Gómez, G. Caracterización de Algunas Propiedades Físicas y Factores de Conversión Del Café Durante El Proceso de Beneficio Húmedo Tradicional. *Cenicafé* **2008**, *59*, 120–142.
47. Moroney, K.M.; O'Connell, K.; Meikle-Janney, P.; O'Brien, S.B.G.; Walker, G.M.; Lee, W.T. Analysing Extraction Uniformity from Porous Coffee Beds Using Mathematical Modelling and Computational Fluid Dynamics Approaches. *PLoS ONE* **2019**, *14*, e0219906. [CrossRef] [PubMed]
48. Mo, C.; Johnston, R.; Navarini, L.; Liverani, F.S.; Ellero, M. Exploring the Link between Coffee Matrix Microstructure and Flow Properties Using Combined X-Ray Microtomography and Smoothed Particle Hydrodynamics Simulations. *Sci. Rep.* **2023**, *13*, 16374. [CrossRef] [PubMed]
49. Duque-Dussán, E.; Sanz-Uribe, J.R.; Dussán-Lubert, C.; Banout, J. Thermophysical Properties of Parchment Coffee: New Colombian Varieties. *J. Food Process Eng.* **2023**, *46*, e14300. [CrossRef]
50. Chen, S.G.; Yang, R.T. Theoretical Basis for the Potential Theory Adsorption Isotherms. In *The Dubinin-Radushkevich and Dubinin-Astakhov Equations*; ACS Publications: Washington, DC, USA, 2002.
51. Golubyatnikov, O.; Akulinin, E. Application of the Dubinin–Radushkevich–Astakhov Equation to Calculate Gases Isotherms on Zeolite Adsorbents (on Example of H2, CO2, CO, CH4, N2 Adsorption on 13X and 5A). *Sep. Sci. Technol.* **2022**, *57*, 2871–2884. [CrossRef]
52. Oh, H.-T.; Lim, S.-J.; Kim, J.H.; Lee, C.-H. Adsorption Equilibria of Water Vapor on an Alumina/Zeolite 13X Composite and Silica Gel. *J. Chem. Eng. Data* **2017**, *62*, 804–811. [CrossRef]
53. Savelli, F.; Socci, L.; Rocchetti, A.; Lippi, M.; Talluri, L. Modelling of a Desiccant-Coated Heat and Mass Exchanger for Airflow Dehumidification in HVAC Systems. *Sustain. Energy Technol. Assess.* **2025**, *82*, 104484. [CrossRef]
54. Van Kampen, J.; Boon, J.; Van Sint Annaland, M. Steam Adsorption on Molecular Sieve 3A for Sorption Enhanced Reaction Processes. *Adsorption* **2021**, *27*, 577–589. [CrossRef]
55. Dayananda, M.A. A Direct Derivation of Fick's Law from Continuity Equation for Interdiffusion in Multicomponent Systems. *Scr. Mater.* **2022**, *210*, 114430. [CrossRef]
56. Strong, C.; Carrier, Y.; Handan Tezel, F. Experimental Optimization of Operating Conditions for an Open Bulk-Scale Silica Gel/Water Vapour Adsorption Energy Storage System. *Appl. Energy* **2022**, *312*, 118533. [CrossRef]
57. Duque-Dussán, E.; Banout, J. Improving the Drying Performance of Parchment Coffee Due to the Newly Redesigned Drying Chamber. *J. Food Process Eng.* **2022**, *45*. [CrossRef]
58. Duque-Dussán, E.; Villada-Dussán, A.; Roubík, H.; Banout, J. Modeling of Forced and Natural Convection Drying Process of a Coffee Seed. *J. ASABE* **2022**, *65*, 1061–1070. [CrossRef]
59. Coradi, P.C.; Martens, S.; Rodrigues, H.E.; Leal, A.F.; Costa, D.R.d.; Saath, R.; Borém, F.M. Development and Validation of a Heated Drying Air Diffusion System to Optimize Rotary Dryers and Final Coffee Quality. *PLoS ONE* **2021**, *16*, e0251312. [CrossRef]
60. Fabbri, A.; Cevoli, C.; Alessandrini, L.; Romani, S. Numerical Modeling of Heat and Mass Transfer during Coffee Roasting Process. *J. Food Eng.* **2011**, *105*, 264–269. [CrossRef]
61. Chilev, C.; Dicko, M.; Langlois, P.; Lamari, F. Modelling of Single-Gas Adsorption Isotherms. *Metals* **2022**, *12*, 1698. [CrossRef]
62. Ahsan, S.; Ayub, A.; Meeroff, D.; Jahandar Lashaki, M. A Comprehensive Comparison of Zeolite-5A Molecular Sieves and Amine-Grafted SBA-15 Silica for Cyclic Adsorption-Desorption of Carbon Dioxide in Enclosed Environments. *Chem. Eng. J.* **2022**, *437*, 135139. [CrossRef]

63. Cavalcanti-Mata, M.E.; Duarte, M.E.; Tolentino, M.; Mendes, F.A.; Batista, L.; De Lima, J.M.; Lúcio, A.; Nascimento, A.P.; Almeida, R.D.; Lisboa, H.M. Drying Kinetics of Industrial Pineapple Waste: Effective Diffusivity and Thermodynamic Properties Resulting from New Mathematical Models Derived from the Fick Equation. *Processes* **2024**, *12*, 1198. [CrossRef]
64. Jakkaew, P.; Yingchutrakul, Y.; Aunsri, N. A Data-Driven Approach to Improve Coffee Drying: Combining Environmental Sensors and Chemical Analysis. *PLoS ONE* **2024**, *19*, e0296526. [CrossRef]
65. Choi, Y.; Cho, W.; Ozaki, A.; Lee, H. Influence of the Moisture Driving Force of Moisture Adsorption and Desorption on Indoor Hygrothermal Environment and Building Thermal Load. *Energy Build.* **2021**, *253*, 111501. [CrossRef]
66. Fauzi, M.B.; Kosasih, E.A.; Dzaky, M.I.; Prabowo, A.T. Effects of Drying Temperature and Specific Humidity on Drying Rate Constant and Activation Energy of Robusta Coffee. *AIP Conf. Proc.* **2024**, *3090*, 060011. [CrossRef]
67. Cam, I.B.; Basunal Gulmez, H.; Eroglu, E.; Topuz, A. Strawberry Drying: Development of a Closed-Cycle Modified Atmosphere Drying System for Food Products and the Performance Evaluation of a Case Study. *Dry. Technol.* **2018**, *36*, 1460–1473. [CrossRef]
68. Zhang, X.; Chen, M.; Guan, J. Regeneration Behavior of Solid Desiccants with Microwave Drying. *J. Therm. Anal. Calorim.* **2024**, *149*, 10927–10940. [CrossRef]
69. Misha, S.; Mat, S.; Ruslan, M.H.; Sopian, K. Review of Solid/Liquid Desiccant in the Drying Applications and Its Regeneration Methods. *Renew. Sustain. Energy Rev.* **2012**, *16*, 4686–4707. [CrossRef]
70. Faraldo, F.; Byrne, P. A Review of Energy-Efficient Technologies and Decarbonating Solutions for Process Heat in the Food Industry. *Energies* **2024**, *17*, 3051. [CrossRef]
71. Méndez Rodríguez, C.; Salazar Benítez, J.; Rengifo Rodas, C.F.; Corrales, J.C.; Figueroa Casas, A. A Multidisciplinary Approach Integrating Emergy Analysis and Process Modeling for Agricultural Systems Sustainable Management—Coffee Farm Validation. *Sustainability* **2022**, *14*, 8931. [CrossRef]
72. Garcia-Freites, S.; Röder, M.; Thornley, P. Environmental Trade-Offs Associated with Bioenergy from Agri-Residues in Sub-Tropical Regions: A Case Study of the Colombian Coffee Sector. *Biomass Bioenergy* **2020**, *140*, 105581. [CrossRef]
73. Zhang, Y.; Chen, Y.; Luo, J.; Yang, H. Improving Air Conditioning Efficiency Using Solar-Assisted Liquid Desiccant Systems: Experimental and Simulation Analysis of Two Desiccants. *Renew. Energy* **2025**, *253*, 123572. [CrossRef]
74. Rashidi, M.; Arabhosseini, A.; Samimi-Akhijahani, H.; Kermani, A.M. Acceleration the Drying Process of Oleaster (*Elaeagnus angustifolia* L.) Using Reflectors and Desiccant System in a Solar Drying System. *Renew. Energy* **2021**, *171*, 526–541. [CrossRef]
75. Metrane, A.; Delhali, A.; Ouikhalfan, M.; Assen, A.H.; Belmabkhout, Y. Water Vapor Adsorption by Porous Materials: From Chemistry to Practical Applications. *J. Chem. Eng. Data* **2022**, *67*, 1617–1653. [CrossRef]
76. Kim, H.; Hong, S.K.; Kang, J.G.; Moon, S.-W.; Kim, G.; Yoon, S.; Wei, D.; Moon, H.; Kim, B.S. Exploration Adsorption Characteristics of Zeolite 13X Depending on Humidity and Flow Rate in Sorption Thermal Energy Storage Applications. *Int. J. Heat. Mass. Transf.* **2024**, *221*, 125049. [CrossRef]
77. Yang, K.; Su, B.; Shi, L.; Wang, H.; Cui, Q. Adsorption Mechanism and Regeneration Performance of 13X for H_2 S and SO_2. *Energy Fuels* **2018**, *32*, 12742–12749. [CrossRef]
78. Liu, L.; Kubota, M.; Li, J.; Kimura, H.; Bai, Y.; Wu, R.; Deng, L.; Huang, H.; Kobayashi, N. Comparative Study on the Water Uptake Kinetics and Dehumidification Performance of Silica Gel and Aluminophosphate Zeolites Coatings. *Energy* **2022**, *242*, 122957. [CrossRef]
79. Al-Ghamdi, S.; Alfaifi, B.; Elamin, W.; Lateef, M.A. Advancements in Coffee Manufacturing: From Dehydration Techniques to Quality Control. *Food Eng. Rev.* **2024**, *16*, 513–539. [CrossRef]
80. Abreu, D.J.M.d.; Lorenço, M.S.; Machado, G.G.L.; Silva, J.M.; de Azevedo, E.C.; Carvalho, E.E.N. Influence of Drying Methods on the Post-Harvest Quality of Coffee: Effects on Physicochemical, Sensory, and Microbiological Composition. *Foods* **2025**, *14*, 1463. [CrossRef] [PubMed]
81. Kazama, E.H.; da Silva, R.P.; de Tavares, T.O.; Correa, L.N.; de Lima Estevam, F.N.; de Nicolau, F.E.A.; Maldonado Júnior, W. Methodology for Selective Coffee Harvesting in Management Zones of Yield and Maturation. *Precis. Agric.* **2021**, *22*, 711–733. [CrossRef]
82. Ronchi, C.P.; DaMatta, F.M. Chapter Thirteen—Managing the Coffee Crop for Flowering Synchronisation and Fruit Maturation: Agronomic and Physiological Issues. In *Advances in Botanical Research*; Damatta, F.M., Ramalho, J.C., Eds.; Coffee—A Glimpse into the Future; Academic Press: Cambridge, MA, USA, 2025; Volume 114, pp. 421–454.
83. Xu, Z.; Aili, T.; Yang, J.; Liu, Y.; Yue, H. Grape Drying Promote Agentia: Food Safety Assessment of a Broad-Spectrum Use Drying Agent for Dried Fruits. *Ecotoxicol. Environ. Saf.* **2025**, *298*, 118204. [CrossRef]
84. Patel, G.; Prudhvi, P.V.V.P.; Patra, A.; Pathak, S.S.; Sonawane, A.D.; Shirkole, S.S. Different Parameters Affecting the Efficiency of Dryers. In *Drying Technology in Food Processing*; Jafari, S.M., Malekjani, N., Eds.; Woodhead Publishing: Cambridge, UK, 2023; pp. 705–742, ISBN 978-0-12-819895-7.
85. Majumder, P.; Deb, B.; Gupta, R. Design and Development of Solar Assisted Fluidized Bed Dryer Integrated with Liquid Desiccant Dehumidifier: Theoretical Analysis and Experimental Investigation. *Energy Convers. Manag.* **2022**, *270*, 116281. [CrossRef]

86. He, F.; Yang, W.; Huang, S.; Wang, X.; Yan, B.; Zhao, X. Moisture Adsorption Performance Investigation on Double Layer Multi-Stage Desiccant Packed Bed under Different Conditions. *Energy* **2025**, *324*, 135994. [CrossRef]
87. Behede, B.; Chakrabarti, S.; Wankhede, U.; Thakare, H. Review on Nanoporous Inorganic Desiccant Materials in the Context of Application in Rotary Dehumidifiers. *Mater. Today Proc.* **2022**, *57*, 2174–2179. [CrossRef]
88. Amani, M.; Bahrami, M. Greenhouse Dehumidification by Zeolite-Based Desiccant Coated Heat Exchanger. *Appl. Therm. Eng.* **2021**, *183*, 116178. [CrossRef]
89. Baruah, N.; Prasanna Kumar, G.V.; Khobragade, C.B. Desiccant Dehumidification: A Potential Method for Different Drying and Cooling Applications. *Russ. J. Phys. Chem. B* **2022**, *16*, 1151–1163. [CrossRef]
90. Suvana, S.; Singh, V.K. Sustainable Green Energy for Enhanced Agricultural Productivity. In *Modern Technology for Sustainable Agriculture*; Kumar, A., Singh, V.K., Singh, Y., Singh, S.K., Kumar, P., Eds.; Springer Nature Switzerland: Cham, Switzerland, 2025; pp. 151–168, ISBN 978-3-031-88396-5.
91. Shimpy; Kumar, M.; Kumar, A. Designs, Performance and Economic Feasibility of Domestic Solar Dryers. *Food Eng. Rev.* **2023**, *15*, 156–186. [CrossRef]